Development/Plasticity/Repair

Human Embryonic Stem Cell-Derived Oligodendrocyte Progenitor Cell Transplants Remyelinate and Restore Locomotion after Spinal Cord Injury

Hans S. Keirstead,[1] Gabriel Nistor,[1] Giovanna Bernal,[1] Minodora Totoiu,[1] Frank Cloutier,[1] Kelly Sharp,[1] and Oswald Steward[1,2,3]

Departments of [1]Anatomy and Neurobiology, [2]Neurobiology and Behavior, and [3]Neurosurgery, Reeve-Irvine Research Center, College of Medicine, University of California at Irvine, Irvine, California 92697-4292

Demyelination contributes to loss of function after spinal cord injury, and thus a potential therapeutic strategy involves replacing myelin-forming cells. Here, we show that transplantation of human embryonic stem cell (hESC)-derived oligodendrocyte progenitor cells (OPCs) into adult rat spinal cord injuries enhances remyelination and promotes improvement of motor function. OPCs were injected 7 d or 10 months after injury. In both cases, transplanted cells survived, redistributed over short distances, and differentiated into oligodendrocytes. Animals that received OPCs 7 d after injury exhibited enhanced remyelination and substantially improved locomotor ability. In contrast, when OPCs were transplanted 10 months after injury, there was no enhanced remyelination or locomotor recovery. These studies document the feasibility of predifferentiating hESCs into functional OPCs and demonstrate their therapeutic potential at early time points after spinal cord injury.

Key words: **predifferentiation; transplantation; acute; chronic; remyelination; functional recovery; rat**

Introduction

The limited regenerative capacity of the adult CNS has directed the focus of preclinical trauma research on means of reducing secondary degeneration and promoting regeneration. Neural stem cells could potentially address both of these needs to benefit the outcome of CNS injury by promoting survival of host tissue, growth of host tissue, and/or replacement of cells lost as a result of trauma. Embryonic stem cells provide novel prospects for cellular replacement strategies because of their ability to provide seemingly unlimited stem cell numbers *in vitro*, their amenability to genetic engineering, and their broad developmental capacity (Okabe et al., 1996; Brustle et al., 1997; Brustle et al., 1999; Reubinoff et al., 2001; Zhang et al., 2001).

Closed contusion injuries spare axons in the subpial white matter in the vicinity of the impact site (Bunge et al., 1993; Kakulas, 1999), and some of these spared axons lose their myelin sheaths (Totoiu and Keirstead, 2005) as a result of the death of oligodendrocytes (Kakulas, 1999). As a result, action potential propagation is disrupted because of the exposure of voltage-gated potassium channels at the internodes (Nashmi and Fehlings, 2001). Oligodendrocytes also undergo apoptosis at considerable distances from the lesion, which disrupt myelin and action potential propagation by surviving axons. Hence, remyelination enhances action potential conduction (Utzschneider et al., 1994; Waxman et al., 1994) and restores functional deficits (Jeffery and Blakemore, 1997; Jeffery et al., 1999).

Here, we undertook a proof of concept experiment to determine the feasibility and efficacy of using human stem cell derivatives to promote remyelination and functional recovery in the injured adult rat spinal cord. In the present study, human embryonic stem cells (hESCs) were induced to differentiate into high-purity oligodendrocyte progenitor cells (OPCs) before transplantation. This strategy obviates the potential problems posed by the capability of embryonic stem cells to form teratomas after implantation and to differentiate in ways that are determined by environmental signals at the site of implantation, which are difficult or impossible to control. High-purity OPCs were then transplanted into spinal cord injury (SCI) sites in rats 7 d or 10 months after injury. We show that rats receiving OPCs at 7 d after injury exhibited enhanced remyelination and recovery of motor function, whereas rats that received OPCs at 10 months did not. These studies demonstrate for the first time that derivatives of hESCs have therapeutic potential for spinal cord injury and indicate that there may be a limited therapeutic window for this treatment.

Materials and Methods

Cell culture. The H7 and H7-enhanced green fluorescent protein (eGFP) hESC lines at passage 32 and the human fibroblast (hFb) line at passage

Received Sept. 22, 2004; revised March 28, 2005; accepted March 30, 2005.

This work was supported by the Geron Corporation, the University of California Discovery Grant, the Roman Reed Spinal Cord Injury Research Fund of California, Research for Cure, and individual donations to the Reeve-Irvine Research Center. F.C. holds a postdoctoral fellowship grant from the Spinal Research Foundation and The Ron Shapiro Charitable Foundation. We thank Jane Lebkowski, Catherine Priest, and Scott Thies for discussion and advice. We thank DoQuyen Huynh, Josh Kunellis, Charlie Mendoza, and Julio Espinosa for assistance with animal care.

Correspondence should be addressed to Dr. Hans S. Keirstead, Department of Anatomy and Neurobiology, Reeve-Irvine Research Center, 2111 Gillespie Neuroscience Research Facility, College of Medicine, University of California at Irvine, Irvine, CA 92697-4292. E-mail: hansk@uci.edu.

DOI:10.1523/JNEUROSCI.0311-05.2005

 0270-6474/05/254694-12$15.00/0

48 were obtained from Geron (Menlo Park, CA). Cells were expanded in hESC growth media (Carpenter et al., 2001) and differentiated (Nistor et al., 2005) according to published protocols. Dissociated cells were placed for 2 d in 50% hESC growth media and 50% glial restriction media (GRM). GRM consisted of DMEM:F-12, B27 supplement (Invitrogen, Carlsbad, CA), 25 μg/ml insulin, 6.3 ng/ml progesterone, 10 μg/ml putrescin, 50 ng/ml sodium selenite, 50 μg/ml holotransferin, 40 ng/ml tri-iodo-thyroidin, 4 ng/ml basic FGF (bFGF), and 10 ng/ml epidermal growth factor (EGF) (Sigma-Aldrich, St. Louis, MO). Cells were then exposed to transition media supplemented with 2 ng/ml bFGF, 20 ng/ml EGF (Sigma-Aldrich), and 10 μM/ml all-trans-retinoic acid (RA) (Sigma-Aldrich) in DMSO (Sigma-Aldrich) for 1 d.

This media was then replaced with 100% GRM supplemented with 20 ng/ml EGF (Sigma-Aldrich) and 10 μM/ml all-trans-RA in DMSO for an additional 7 d. RA was then omitted from media for the duration of the differentiation protocol. Cells were exposed to GRM supplemented with 20 ng/ml EGF for 25 d. At day 28, cultures of floating yellow spheres were plated in T75 flasks coated with 1:30 Matrigel for 1 week. Cultures were then exposed to trypsin-EDTA (Invitrogen) for 2–5 min, plated on 1:30 Matrigel substrate, and cultured for 1 week in GRM supplemented with 20 ng/ml EGF. Thus, the differentiation protocol took 42 d.

For terminal differentiation and immunocytochemical staining, OPCs were plated on poly-L-lysine- and human laminin- (Sigma-Aldrich) coated slides. Media was changed every other day. For transplantation, cells were exposed to 1:5000 2′,3′-bromodeoxyuridine for 3 d or 1:5000 bisbenzimide for 10 min and then concentrated to 100,000 cells/μl. Trypan blue exclusion testing indicated that this preparation consisted of 87–98% viable cells.

Immunocytochemical staining. Nuclear staining was conducted by exposing cultures to Mayer's hematoxylin. Immunostaining using primary antiserum containing mouse anti-O4 (1:50), rabbit anti-galactocerebroside (GalC; 1:200), mouse anti-receptor-interacting protein (RIP; 1:100), rabbit anti-NG2 (1:100), rabbit anti-SOX10 (1:200), rabbit anti-bone morphogenetic protein 4 (BMP4; 1:100), rabbit anti-Olig1 (1:200), mouse anti-A2B5 (1:100) (all from Chemicon, Temecula, CA), mouse anti-class III β-tubulin (Tuj1; 1:200), rabbit anti-Pax6 (1:100) (all from Covance Research Products, Denver, PA), rabbit anti-cow GFAP (1:500; DakoCytomation, Glostrup, Denmark), and mouse anti-stage-specific embryonic antigen 4 (SSEA4) supernatant (1:5; gift from Geron) was conducted using standard protocols. The percentage of immunopositive cells was determined by dividing the total number of immunopositive cells by the total number of hematoxylin-positive cells in each imaging chamber and averaging the results from three imaging chambers per marker.

Experimental groups. To determine whether OPCs are capable of restoring myelin and improving motor function when transplanted at a short interval after SCI, 1.5 million OPCs were transplanted into the spinal cord 7 d after a contusion injury at the thoracic level (200 kdyn force; $n = 8$). This injury is moderate in severity, sparing some hindlimb motor function, but severely impairs hindlimb use during overground locomotion. All histological data presented for acute transplants pertain to this experimental group. Acute transplantation controls included animals that received an equivalent number of hFbs ($n = 8$) or vehicle-only injections ($n = 8$) 7 d after a 200 kdyn SCI. After demonstrating that transplanted OPCs enhance remyelination in the acute transplant group (see below), we then determined in a separate experiment whether the transplanted cells were responsible for remyelination by transplanting eGFP-expressing, hESC-derived OPCs ($n = 8$) 7 d after a 200 kdyn SCI. After demonstrating that transplanted OPCs improve locomotion in the acute transplant group (see below), we then determined in a separate experiment whether fewer OPCs (250,000 cells) could elicit the same behavioral effect ($n = 8$); acute transplant controls for this experiment included animals that received vehicle-only injections ($n = 8$).

To determine whether OPCs are capable of restoring myelin and improving motor function when transplanted at a long interval after SCI, 1.5 million OPCs were transplanted into the spinal cord 10 months after a contusion injury at the thoracic level (200 kdyn force; $n = 6$). All histological data presented for chronic transplants pertain to this experimental group. Chronic transplantation controls included animals that received vehicle-only injections ($n = 6$) 10 months after a 200 kdyn SCI. After demonstrating that transplanted OPCs do not benefit SCI in the chronic transplant group (see below), we then determined in separate experiments whether a lack of behavioral effect was also evident for injuries of different levels of severity (150 kdyn, $n = 6$; 250 kdyn, $n = 6$); chronic transplant controls for these experiments included animals that received vehicle-only injections (150 kdyn study, $n = 6$; 250 kdyn study, $n = 6$).

Spinal cord injury. Female Sprague Dawley adult rats (200–220 g; 6–8 weeks of age) were anesthetized with an intraperitoneal injection of 7.5 mg/kg ketamine (Phoenix Pharmaceutical, St. Joseph, MO) and 60 mg/kg xylazine (Phoenix Pharmaceutical). The dorsal area between the neck and hindlimbs and extending ~2 cm bilaterally from the spine was shaved and disinfected with serial provodone and 70% ethanol scrubs. A midline incision exposed the spinal column at the level of T8–T11, and the paravertebral muscles were dissected bilaterally to visualize the transverse apophyses. Laminectomy was performed at T10. Contusion injury was induced using the Infinite Horizon Impactor (Precision Systems, Kentucky, IL) with a force of 150, 200, or 250 kdyn. The Infinite Horizon Impactor delivers a sudden impact of a desired force to the exposed spinal cord of a rat suspended by clamps on the vertebrae cranial and caudal to the laminectomy. The deep and superficial muscle layers were sutured, and the skin was closed with stainless-steel wound clips. Immediately after surgery, animals were given subcutaneous saline and prophylactic Baytril (2.5 mg/kg/d, s.c.; Bayer, Shawnee Mission, KS) and maintained on an isothermic pad until alert and mobile. Animals received manual bladder expression twice daily and were inspected for weight loss, dehydration, discomfort, and autophagia, with appropriate veterinary care as needed.

Behavioral testing. Before injury, each animal was acclimated and scored using the Basso, Beattie, Bresnahan Locomotor Rating Scale (BBB) (Basso et al., 1995) and four-parameter kinematic analyses (Gonzalez et al., 2003). BBB scores were analyzed by repeated measures ANOVA with Tukey's multiple comparison test at each time point. For kinematic analyses, animals were videotaped using a Hitachi 8 mm video camcorder (VM-E555LA; Hitachi, Tokyo, Japan) from underneath Plexiglas bearing defined 1cm grid lines. The videos were analyzed frame by frame using FMV 2.0 software and scored independently by two observers blinded to the treatment group. Rear paw stride length was defined as distance from the start of a step with the rear paw through to the end of that step with the same paw (measurements taken on each side for three consecutive steps and averaged). Stride width was defined as the distance from the left outermost hindpaw digit to the right outermost hindpaw digit. Toe spread was defined as the distance from the most lateral point of the lateral digit to the most medial point of the medial digit of the hindpaws. Paw rotation was defined as the angle between the axis of the rear paws and the midline axis of the body in degrees. The SPSS 11.5 *t* test (SPSS, Chicago, IL) was used to determine differences between treated and untreated groups.

Cell transplantation. Animals received cyclosporin A (10 mg/kg/d, s.c.; Bedford Laboratories, Bedford, OH) beginning 1 d before transplantation until the end of the study. Transplantation surgeries occurred 7 d or 10 months after contusion surgery. Immediately before transplant, the cell transplant population was assayed for viability by assessing trypan blue exclusion, and only populations with >95% viability were transplanted. Animals were anesthetized as above, and the laminectomy site was re-exposed. After immobilization of the spinal process rostral to the contusion site, a 10 μl Hamilton syringe (Hamilton, Reno, NV) with a silicon-coated pulled glass tip was lowered into the spinal cord using a stereotactic manipulator arm. Cell suspensions were injected along the midline of the spinal cord at a depth of 1.2 mm into one site 4 mm cranial to the lesion epicenter and one site 4 mm caudal to the lesion epicenter, in a total volume of either 2.5 μl (250,000 cells) or 15 μl (1,500,000 cells) at a rate of 2 μl/min. Animals in which the injected solution was seen to exit from the needle track during injection or after withdrawal of the needle were omitted from the experiment (and are not represented in the experimental numbers). The host spinal cord cranial and caudal to the lesion epicenter was targeted to avoid the epicenter of cavitation, hemorrhagic

necrosis, and inflammation, which might decrease cell survival and integration and to target the penumbra of the lesion, which has been shown to contain regions of demyelination (Totoiu and Keirstead, 2005). The needle was removed after 5 min. Control animals received either hFbs at similar concentrations or DMEM vehicle only.

Histology. Animals were killed 8 weeks after cell transplantation under pentobarbitone anesthesia by aortic perfusion with 4% glutaraldehyde (Fisher Scientific, Pittsburgh, PA) in 0.1 M phosphate buffer, pH 7.4, for resin processing or 4% paraformaldehyde (Fisher Scientific) in 0.1 M phosphate buffer, pH 7.4, for cryostat processing. Resin sections were used to determine the number of remyelinated axons and the gross pathology of the transplant environment. Cryostat sections were used to determine the spread of bromodeoxyuridine (BrdU) and bisbenzimide-prelabeled transplanted cells, the distribution of anti-human immunostained cells, the differentiation profile of transplanted cells, and morphometric assessments of tissue sparing/loss.

For resin processing, the length of the spinal cord extending 2–3 mm caudal to the injury epicenter was dissected and postfixed for 24 h in 4% glutaraldehyde (Fisher Scientific) and then exposed to 1% OsO_4 (Electron Microscopy Sciences, Fort Washington, PA), dehydrated in ascending alcohols, and embedded in Spurr resin (Electron Microscopy Sciences) according to standard protocols. Transverse semithin (1 μm) sections were cut from the rostral face, stained with alkaline toluidine blue, coverslipped, and examined by light microscopy on an Olympus (Tokyo, Japan) AX-80 microscope using Olympus MicroSuite B3SV software. For electron microscopy, blocks were trimmed and sections were cut at 100 nm, mounted on copper grids, uranyl acetate and lead citrate stained, and viewed under a Hitachi EM 600 electron microscope at 75 kV.

To quantify normally myelinated, demyelinated, and oligodendrocyte or Schwann cell-remyelinated axons, regions of pathology on 1 μm resin sections were located at 200× magnification and traced using the Olympus MicroSuite B3SV software (Olympus America, Melville, NY) to calculate area. Images of these regions were digitally captured at 2000× magnification, and a 25 × 25 μm (625 μm^2) digital grid was overlaid on the images using Olympus MicroSuite B3SV software (Olympus America). Normally myelinated, demyelinated, and oligodendrocyte or Schwann cell-remyelinated axons were counted on five 625 μm^2 areas aligned on a radial oriented line, according to the line-sampling technique outlined by Blight (1983). The radial oriented line originated at the central canal and radiated to the outermost limit of the spinal cord cross section through the middle of the area of pathology; in the absence of a central canal, the radial oriented line originated at the intersection of two digitally imposed lines, one line running from the outermost center point of the dorsal column to the outermost center point of the ventral column and the other line spanning the greatest mediolateral width of the spinal cord. The 625 μm^2 areas were then superimposed on this radial oriented line. The number of normally myelinated, demyelinated, and oligodendrocyte or Schwann cell-remyelinated axons was determined by counting axons in each 625 μm^2 region, averaging the number of axons within all of the 625 μm^2 regions along the radial line and then multiplying this number by the area measurement of the region of pathology through which the radial line traversed and dividing by 625. This calculation yielded an estimate of the total number of axons within a region of pathology. The number of normally myelinated, demyelinated, and oligodendrocyte or Schwann cell-remyelinated axons was similarly determined for all regions of pathology on the tissue section, summed, and presented as number of axons per square millimeter.

Demyelinated axons were identified by the absence of a myelin sheath around axons free from vesicles or dense body accumulation. Oligodendrocyte-remyelinated axons were identified by their characteristically thin myelin sheaths relative to the diameter of the axons, with a myelin sheath thickness ranging from 0.1 to 0.4 μm (Hildebrand and Hahn, 1978; Guy et al., 1989; Gilson and Blakemore, 2002). Schwann cell-remyelinated axons were identified by their characteristically thick myelin sheaths relative to axon diameter, with myelin sheath thickness ranging from 0.6 to 1.2 μm, their darker myelin staining relative to oligodendrocyte myelin, and the presence of a cell body immediately juxtaposed to the myelin sheath (Hildebrand and Hahn, 1978; Guy et al., 1989; Gilson and Blakemore, 2002). Normal oligodendrocyte-myelinated axons were identified by their characteristically thick myelin sheaths relative to the diameter of the axons, with a myelin sheath thickness ranging from 1.0 to 1.8 μm (Hildebrand and Hahn, 1978; Guy et al., 1989; Gilson and Blakemore, 2002). G-ratios (myelin sheath thickness/axon diameter) were determined for randomly selected oligodendrocyte- or Schwann cell-remyelinated axons within the same 625 μm^2 areas of pathology used for axon quantification (above). Random sampling was accomplished by measuring the G-ratio for only those axons bisected by horizontal grid lines digitally superimposed on 2000× digitally captured images. Measurements of myelin sheath thickness and axon diameter were conducted using Olympus MicroSuite B3SV software (Olympus America) on digitally captured images magnified to 4000×.

For cryostat processing, dissected spinal cords were cryoprotected in a 30% sucrose solution in PBS, and the lengths of spinal cord extending 12 mm cranial and caudal to the lesion epicenter were frozen sectioned in the trans-

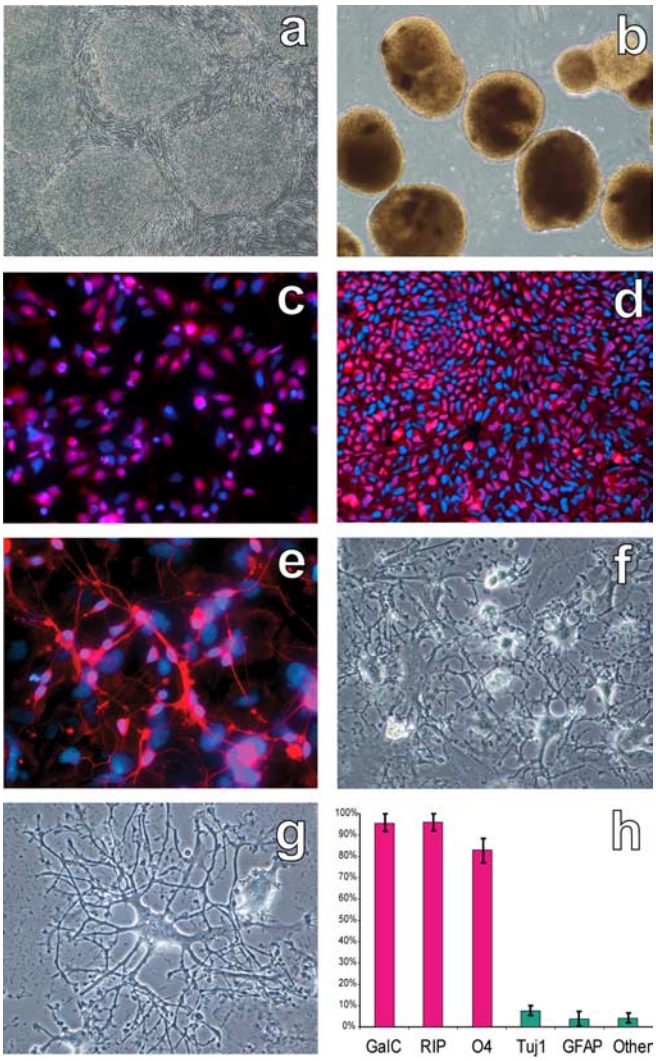

Figure 1. Commitment of hESCs to oligodendrocyte progenitors. ***a***, Undifferentiated hESCs readily expand in colonies, separated by stromal cells. ***b***, Yellow spheres appeared within 5 d of exposure to RA and grew rapidly in the presence of GRM, evidenced by an increase in their size and proportion relative to other culture components. ***c***, A total of 83 ± 7% of cells expressed the transcription factor Olig1 (red) associated with oligodendrocyte and motoneuron specification. ***d***, A total of 72 ± 12% of cells expressed the DNA binding protein SOX10 (red) expressed within oligodendrocyte precursors. ***e***, More than 95% of cells labeled with the mature oligodendroglial marker RIP (red). Cells that did not label with oligodendroglial markers were primarily GFAP positive or Tuj1 positive. ***f***, ***g***, Plated cells adopted a typical oligodendroglial morphology characterized by multiple branches. ***h***, Quantitation of immunolabeling. Error bars illustrate SD. Magnification: ***a***, 50×; ***c***, ***d***, 100×; ***e***, ***f***, 200×; ***b***, ***g***, 400×.

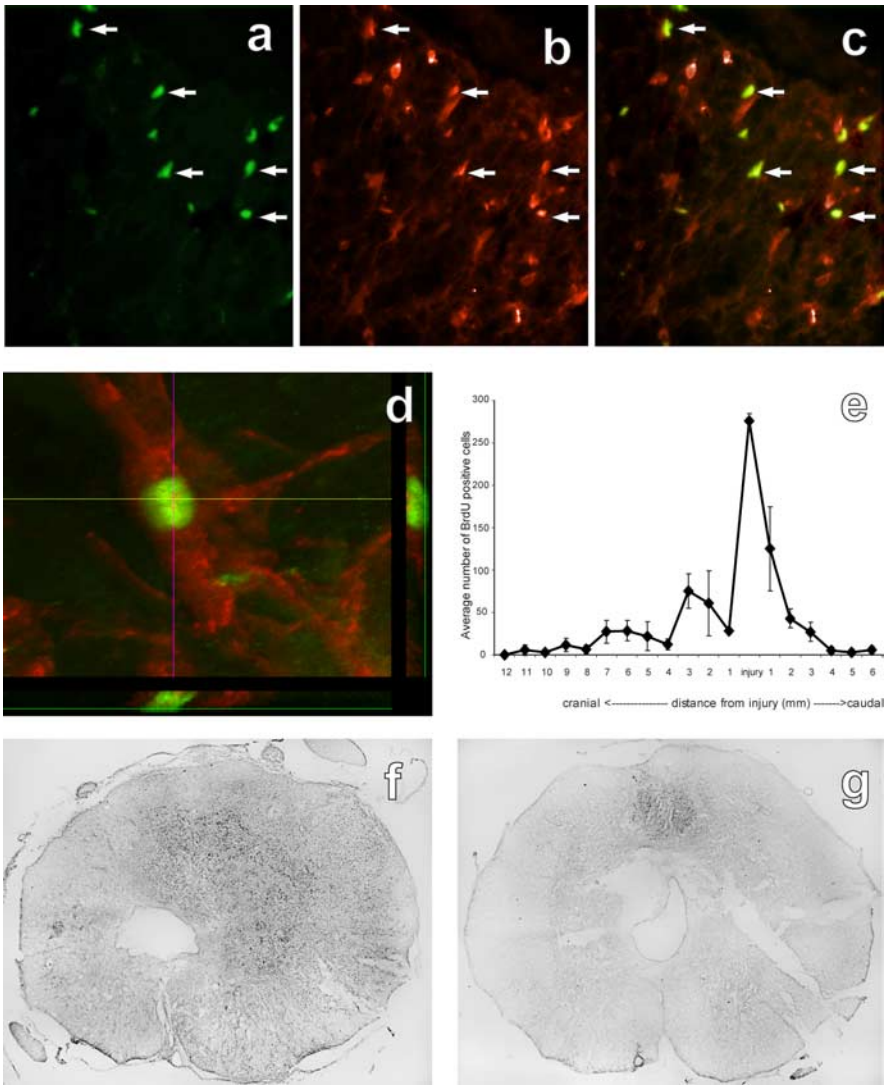

Figure 2. Acute transplantation of hESC-derived OPCs resulted in cell survival, limited redistribution from the site of implantation, and differentiation to mature oligodendrocytes. ***a***, Anti-human nuclei-positive OPCs (arrows) double labeled with the mature oligodendrocyte marker APC-CC1 (arrows; ***b***); a composite is shown in ***c***. ***d***, Anti-human nuclei-positive, APC-CC1-positive double labeling was confirmed using 3-D reconstruction of confocally scanned thin-plane images. ***e***, Distribution of total numbers of BrdU-prelabeled cells within spinal cord transverse sections 2 months after transplantation at 7 d after SCI. Error bars illustrate SD. ***f***, Anti-human nuclei-immunostained transverse section 1 mm caudal to the site of implantation showing transplanted cells (black dots) located primarily within the gray matter but also redistributed throughout the white matter. ***g***, Anti-human nuclei-immunostained transverse section 6 mm cranial to the site of implantation, showing transplanted cells (black dots) located primarily within the dorsal column. Magnification: ***a–c***, 400×; ***d***, 2000×; ***f***, ***g***, 20×.

verse plane at 20 μm. Immunostaining using primary antiserum containing mouse anti-human nuclei (1:30; Chemicon), mouse anti-BrdU (1:200; Accurate Chemical, Westbury, NY), rabbit anti-cow GFAP (1:500; DakoCytomation), mouse anti-APC-CC1 (1:200; Oncogene Research Products, San Diego, CA), mouse anti-neuronal-specific nuclear protein (NeuN; 1:200; Chemicon), rabbit anti-green fluorescent protein (1:200; Abcam, Cambridge, UK), and mouse anti-Tuj1 (1:200; Covance, Berkeley, CA) was conducted on sections at 1 mm intervals according to standard protocols. To determine distribution of transplanted cells, the number of immunopositive cells were counted on three sections 80 μm apart from each tissue block for each animal and averaged; the counts within corresponding blocks from animals within a group were then averaged. Double labeling of cells with anti-BrdU+ or anti-human+ nuclei plus cellular differentiation markers was confirmed using confocal microscopy (MRC 1000; Bio-Rad, Hercules, CA; Zeiss, Thornwood, NY). Single confocal plane images of BrdU, human nuclei, or phenotype markers (see above) were collected and combined to produce three-dimensional (3-D) reconstruction and determine label colocalization. To quantify neurofilament-positive axons and GFP-positive profiles surrounding neurofilament-positive axons in animals transplanted with eGFP-expressing hESC-derived OPCs, the line-sampling technique outlined above for axon quantification in resin sections was used. Morphometric analysis of spinal cord size was conducted by tracing tissue sections using Olympus MicroSuite B3SV software to calculate the area on three sections 80 μm apart from each tissue block for each animal and averaged; the measurements within corresponding blocks from animals within a group were then averaged. All cystic enlargements were subtracted from the total area.

Statistical methods. BBB scores were analyzed by repeated measures ANOVA with Tukey's multiple comparison test at each time point. The SPSS 11.5 *t* test was used to determine differences between kinematic scores for treated and untreated groups. The SPSS 11.5 *t* test was used to determine differences between quantitative histological scores.

Results

Generation of OPCs from hESCs

hESC colonies separated by stromal cells were observed within 1 d of cell passage (Fig. 1*a*) and expressed SSEA4, a surface marker for undifferentiated hESCs (Thomson et al., 1998).

The antigenic characterization of OPCs generated for the acute transplant and the chronic transplant is summarized in supplemental Table 1 (available at www.jneurosci.org as supplemental material). For reference, the antigenic characterization from our original derivation of OPCs from hESCs (Nistor et al., 2005) is also presented in supplemental Table 1 (available at www.jneurosci.org as supplemental material). Yellow spheres began to appear within 5 d of exposure to RA (Fig. 1*b*) and increased in size during exposure to GRM. Yellow spheres were composed of oligodendroglial lineage-committed cells. The cell population prepared for the acute transplantation contained 97 ± 3% Pax6-positive cells, and the cell population prepared for the chronic transplantation contained 96 ± 3% Pax6-positive cells. Exceedingly few Pax6-positive cells were present within the periphery of spheres and among the migrating cells immediately adjacent to the spheres. Pax6 expression was present in <1% of cells on day 42 of the differentiation protocol in both the acute and chronic cell preparations. Because Pax6 is a potent neurogenic gene (Heins et al., 2002), this indicates that the majority of undifferentiated cells at early stages of the differentiation protocol are neural progenitors. The cell population prepared for the acute transplantation expressed Olig1 (84 ± 6%) (Fig. 1*c*), SOX10 (76 ± 8%) (Fig. 1*d*), A2B5 (98 ± 2%), and NG2 (97 ± 3%) within the periphery of spheres and immediately adjacent to the spheres, indicating that these neural progenitors adopt an oligodendroglial fate. The cell population prepared for the chronic transplantation exhibited a similar oligodendroglial expression pattern (Olig1, 88 ± 5%; SOX10, 70 ± 13%; A2B5, 95 ± 3%; NG2, 99 ± 1%). This panel of

markers demonstrates oligodendroglial lineage commitment. The cells also had a bipolar morphology, characteristic of immature oligodendroglial cells. No SSEA4-positive cells could be detected at this point in the differentiation protocol for either the acute or chronic preparation, indicating that cultures were devoid of stem cells.

The development of oligodendroglia was confirmed 14 d after plating cells at the end of the differentiation protocol. The cell population prepared for the acute transplantation expressed the oligodendroglial markers GalC (94 ± 6%), RIP (95 ± 5%) (Fig. 1*e*), and O4 (82 ± 7%). The cell population prepared for the chronic transplantation also expressed the oligodendroglial markers GalC (97 ± 2%), RIP (90 ± 6%), and O4 (80 ± 3%). Cells that did not label with oligodendroglial markers were primarily GFAP positive (astrocytes) or Tuj1 positive (neurons) in both the acute (4 ± 2% GFAP; 3 ± 2% Tuj1) and chronic (4 ± 3% GFAP; 5 ± 2% Tuj1) preparations. Double immunostaining indicated that no GFAP- or Tuj1-positive cells coexpressed oligodendroglial markers. No BMP4-positive or SSEA4-positive cells could be detected in either the acute or chronic preparations, indicating that cultures were devoid of mesodermal lineage cells or stem cells. All cells displayed the typical highly branched morphology of oligodendrocytes (Fig. 1*f*,*g*).

OPCs survive and differentiate into oligodendrocytes when transplanted at 7 d after injury

Transplanted prelabeled hESC-derived OPCs survived and redistributed over short distances of the spinal cord during the postimplantation survival period (Fig. 2). Bisbenzimide-positive, BrdU-positive, and anti-human nuclei-positive (Fig. 2*a*) cells were detected in all transplanted animals, confirming survival of transplanted cells. Animals without transplants exhibited no labeling for bisbenzimide, BrdU, or anti-human nuclei. Quantitative analysis indicated that BrdU-positive cells were detected 11 mm cranial and 3 mm caudal to the site of implantation, with the greatest number of cells around the site of implantation and only a modest number of cells redistributed over long distances (Fig. 2*e*).

We assessed whether the transplanted cells retained immunocytochemical markers for oligodendrocytes by double staining spinal cord sections for the oligodendroglial marker APC-CC1 and markers for transplanted cells. Immunostaining identified anti-human nuclei-positive cells (Fig. 2*a*), bisbenzimide-positive cells (data not shown), and BrdU-positive cells (data not shown) that were double labeled with the oligodendroglial marker APC-CC1 (Fig. 2*b*,*c*), indicating that transplanted cells differentiated into oligodendrocytes. Double labeling was confirmed using 3-D reconstruction of confocally scanned thin-plane images (Fig. 2*d*). In almost all instances, these double-labeled cells were found in clusters. Both transplanted and nontransplanted animals also contained APC-CC1-positive cells that were negative for anti-human nuclear antigen, bisbenzimide, and BrdU and were thus endogenous oligodendrocytes. No anti-human nuclei-positive, BrdU-positive, or bisbenzimide-positive cells colabeled with GFAP or NeuN. Anti-human-positive cells were distributed throughout the transverse plane of the spinal cord primarily within the gray matter near the site of implantation (Fig. 2*f*) and within white matter tracts distant from the site of implantation (Fig. 2*g*).

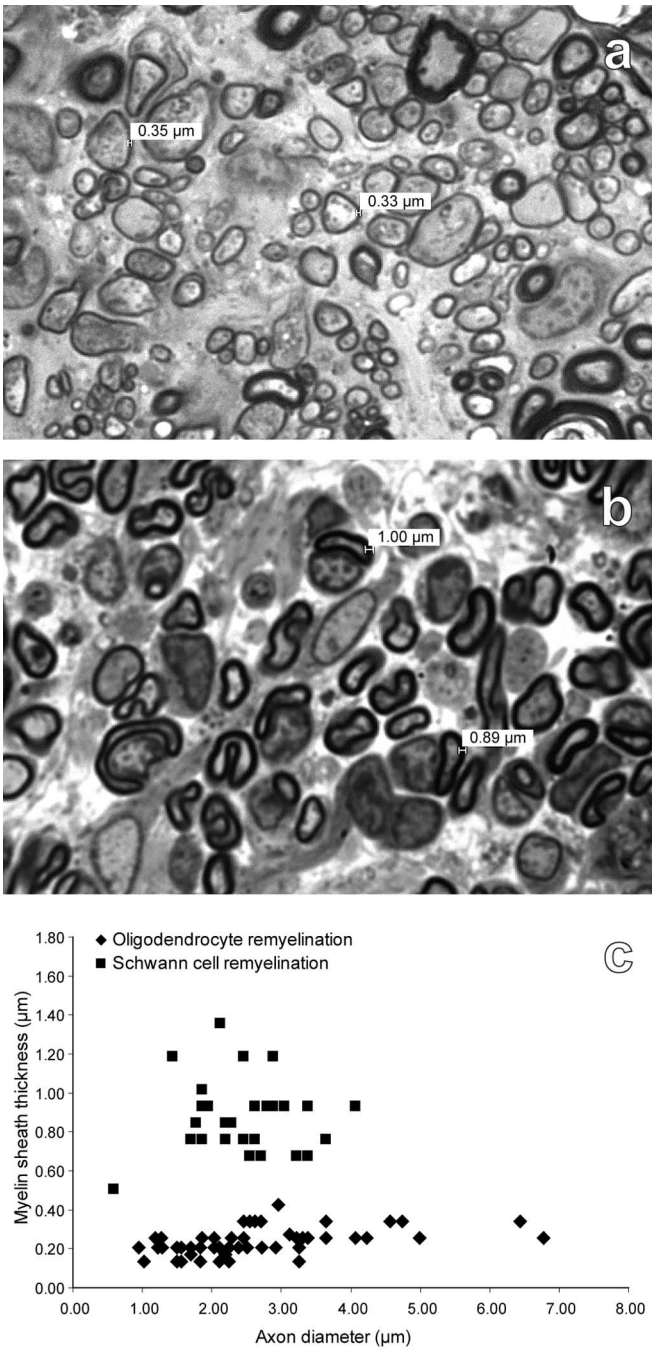

Figure 3. Oligodendrocyte remyelination can be distinguished from Schwann cell remyelination. ***a***, ***b***, Toluidine blue-stained transverse sections of hESC-derived OPC-transplanted animals at the magnification used for quantification, illustrating measurements of the myelin sheath thickness of oligodendrocyte-remyelinated axons (***a***) and Schwann cell-remyelinated axons (***b***). Magnification: ***a***, ***b***, 2000×. ***c***, Myelin sheath thickness against axon diameter in oligodendrocyte-remyelinated and Schwann cell-remyelinated axons. The G-ratio was 10 ± 4 (53)* for oligodendrocyte-myelinated axons and 41 ± 16 (48) for Schwann cell-remyelinated axons. Myelin sheath thickness in axons remyelinated by oligodendrocytes never reached the thickness observed in Schwann cell-remyelinated axons. *, Data are expressed as mean ± SD; the number in parentheses shows the number of axons scored.

Oligodendrocyte remyelination can be distinguished from Schwann cell remyelination

To ensure that oligodendrocyte remyelination could reliably be distinguished from Schwann cell remyelination, we analyzed oligodendrocyte and Schwann cell G-ratios (the ratio between the thickness of the myelin sheath and the diameter of the axon). Oligodendrocyte-remyelinated axons had characteristically thin myelin sheaths relative to the diameter of the axons (Fig. 3*a*). Schwann cell-remyelinated axons had characteristically thick myelin sheaths relative to axon diameter (Fig. 3*b*). Myelin sheath

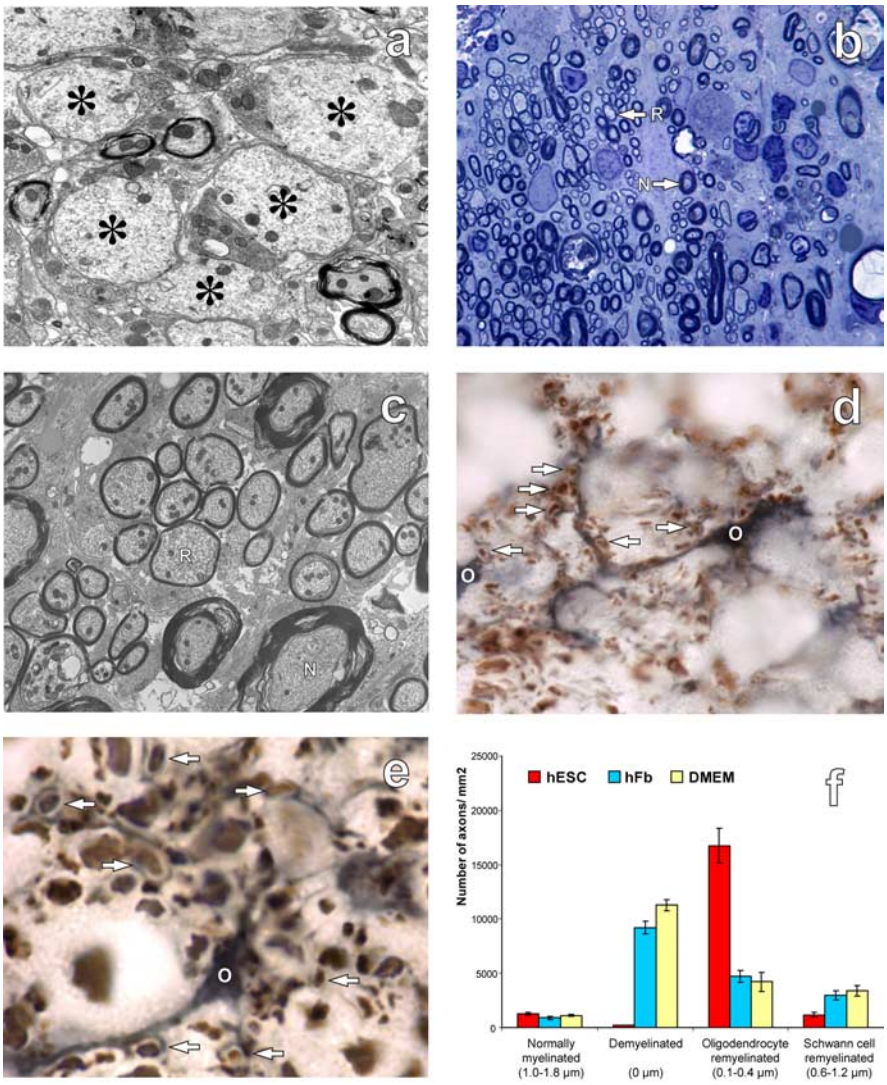

Figure 4. Acute transplantation of hESC-derived OPCs resulted in a significant increase in the density of oligodendrocyte remyelination compared with controls. ***a***, Electron micrograph of the transplant environment at 7 d after injury, illustrating demyelinated axons (*) in an extracellular environment free of astrogliosis. ***b***, Toluidine blue-stained transverse section and electron micrograph (***c***), illustrating robust oligodendrocyte remyelination (R; with characteristically thin myelin sheaths) among few normally myelinated axons (N). ***d***, ***e***, Anti-GFP and anti-neurofilament double immunostains illustrating highly branched GFP-positive OPCs (O) extending processes that ensheath nearby neurofilament-positive axons (arrows), confirming that remyelination was performed by eGFP-labeled transplanted cells. ***f***, Quantification of normally myelinated, demyelinated, and oligodendrocyte or Schwann cell-remyelinated axons in hESC-derived OPC-transplanted, hFb-transplanted, and DMEM-injected animals. Error bars illustrate SD. The myelin sheath thickness for each class of axons is indicated in brackets. Magnification: ***a***, 6000×; ***b***, 400×; ***c***, 3000×; ***d***, 600×; ***e***, 1000×.

thickness in axons remyelinated by oligodendrocytes never reached the thickness observed in Schwann cell-remyelinated axons (Fig. 3*c*). The mean G-ratio of oligodendrocyte-remyelinated axons, 10 ± 4 (53), was significantly less than ($p < 0.01$) the mean G-ratio of Schwann cell-remyelinated axons, 41 ± 16 (48). Data are expressed as mean ± SD; the number in parentheses shows the number of axons scored.

Oligodendrocyte-remyelinated axons appeared in bundles interspersed with normally myelinated axons (Fig. 3*a*). Schwann cell-remyelinated axons were consistently found within the central regions of pathology (Fig. 3*b*). Relatively few Schwann cell-remyelinated axons were found interspersed with normally myelinated or oligodendrocyte-remyelinated axons.

OPCs remyelinate axons when transplanted at 7 d after injury

Electron microscopic analysis of the spinal cord 7 d after injury (i.e., the transplant environment) indicated numerous clusters of demyelinated axons in an extracellular environment free of astrogliosis (Fig. 4*a*), confirming previous studies (Kakulas, 1999; Totoiu and Keirstead, 2005). Eight weeks after OPC or human fibroblast transplantation or DMEM injection, we assessed the extent of normally myelinated, demyelinated, and oligodendrocyte or Schwann cell-remyelinated axons around the injury site. In animals that received OPC transplants, oligodendrocyte remyelinated axons were abundant and typically appeared in aggregates distributed throughout the dorsal, ventral, and lateral columns among few demyelinated and normally myelinated axons (Fig. 4*b*,*c*).

To confirm that the transplanted OPCs performed the remyelination, a separate group of rats received transplants of eGFP-expressing hESC-derived OPCs at 7 d after injury. Two months after transplantation, anti-GFP and anti-neurofilament double immunostaining revealed numerous highly branched GFP-positive cells with a morphology characteristic of oligodendrocytes (i.e., a cell with long processes extending to axons). GFP-positive processes could be seen around neurofilament-positive axons (Fig. 4*d*,*e*), and, in some cases, processes could be followed from a GFP-positive cell body to a region with numerous GFP-positive profiles surrounding NF-positive axons (Fig. 4*d*,*e*).

Quantification of normally myelinated, demyelinated, and oligodendrocyte or Schwann cell-remyelinated axons within the acute transplant group indicated that the density of oligodendrocyte-remyelinated axons was significantly ($p < 0.01$) higher in OPC-transplanted animals compared with hFb-transplanted or DMEM-injected control animals (Fig. 4*f*). OPC-transplanted animals also contained significantly ($p < 0.01$) lower densities of demyelinated and Schwann cell-remyelinated axons when compared with hFb-transplanted or DMEM-injected control animals (Fig. 4*f*). Notably, the total number of oligodendrocyte and Schwann cell remyelinated axons increased from 7592/mm^2 in nontransplanted control animals to 17,908/mm^2 in OPC-transplanted animals (Fig. 4*f*), indicating a 136% increase in remyelination in OPC-transplanted animals. Quantification of neurofilament-positive axons and GFP-positive profiles surrounding neurofilament-positive axons in animals transplanted with eGFP-expressing hESC-derived OPCs (Fig. 4*d*,*e*) indicated that the density of neurofilament-positive axons was 18,111 ± 2420 axons/mm^2, and the density of GFP-positive profiles surrounding axons was 10,018 ± 1580 per mm^2. These data suggest that ~55% of axons were remyelinated

by transplanted GFP-positive oligodendrocytes, although this is likely an underestimate given the poor resolution of immunostained cryosections at high magnification and the difficulties of detecting thin oligodendrocyte remyelination. Axon quantification from high-resolution resin sections (Fig. 3*a*) indicated that oligodendrocyte-remyelinated axons (16,750 ± 1600) represented 87% of the total number of axons (19,356 ± 1952) (Fig. 4*f*) in OPC-transplanted animals. Comparing the percentage of transplant-mediated oligodendrocyte remyelination from the GFP study with the percentage of oligodendrocyte remyelination from the resin study suggests that at least 63% of oligodendrocyte remyelination was performed by the transplanted cells. The density of normally myelinated axons within regions of pathology in the three groups did not differ significantly ($p > 0.1$) (Fig. 4*f*).

OPCs improve motor function when transplanted at 7 d after injury

To determine whether transplantation of OPCs improved recovery of function after SCI, locomotion was assessed using the BBB locomotor scale and four-parameter kinematic analyses. Animals that received OPCs 1 week after SCI exhibited significantly ($p < 0.01$) higher BBB locomotor function scores compared with hFb transplanted or DMEM-injected control animals (Fig. 5*a*,*b*). Importantly, whereas hFb-transplanted or DMEM-injected control animals began to plateau in their locomotor abilities by 2 weeks after injury, OPC-transplanted animals continued to improve their locomotor abilities until ~1 month after injury. OPC-transplanted and control groups did not differ consistently until the fourth testing period after transplantation (12 d after transplantation). After that, OPC-transplanted animals consistently demonstrated significantly ($p < 0.01$) greater locomotor capabilities compared with controls. There was no significant ($p > 0.1$) difference between the locomotor capabilities of injured animals that received transplants of 250,000 OPCs (Fig. 5*a*) and injured animals that received transplants of 1,500,000 OPCs (Fig. 5*b*), although the later group did not begin to exhibit significantly higher locomotor function scores until somewhat later (21 d after transplantation).

Animals that received OPCs 1 week after SCI also exhibited improved motor scores using four-parameter kinematic analyses (grid test). hFb-transplanted or DMEM-injected control animals demonstrated typical deficits, including decreased rear paw stride length and increased rear paw stride width, rear paw toe spread, and rear paw rotation when compared with uninjured control animals (Fig. 5*c*). Animals that received OPCs 1 week after SCI exhibited significantly greater rear paw stride length ($p < 0.01$) and significantly less rear paw stride width ($p < 0.01$), rear paw toe spread ($p < 0.01$), and rear paw rotation ($p < 0.01$) when compared with hFb-transplanted or DMEM-injected control animals at 8 weeks after cell transplantation (Fig. 5*c*). Animals that received OPCs 1 week after SCI exhibited less rear paw stride width, rear paw toe spread, and rear paw rotation when compared with hFb-transplanted or DMEM-injected control animals, although their scores were not significantly different. Rear paw stride length in OPC-transplanted animals was significantly ($p < 0.01$) lower than in uninjured control animals (Fig. 5*c*).

OPCs also survive and differentiate into oligodendrocytes when transplanted at 10 months after injury

When transplants of OPCs were made at 10 months after spinal cord injury, the OPCs again survived and redistributed over short distances of the spinal cord (Fig. 6). Bisbenzimide-positive, BrdU-positive (Fig. 6*a*), and anti-human nuclei-positive cells

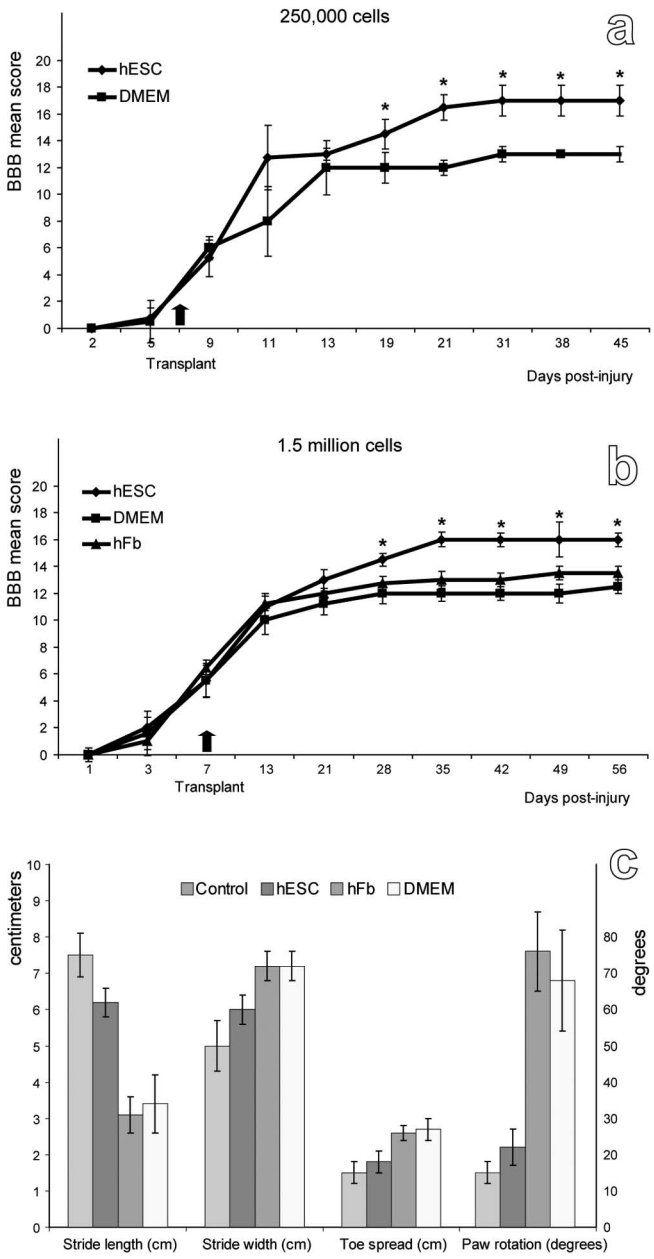

Figure 5. Acute transplantation of hESC-derived OPCs resulted in a significant increase in locomotor recovery compared with controls. ***a***, From ~3 weeks after implantation for the duration of testing, animals that received 250,000 hESC-derived OPCs consistently demonstrated significantly greater locomotor capabilities ($p < 0.01$) compared with controls, as determined using the BBB locomotor rating scale. ***b***, The degree of locomotor recovery in animals that received 1.5 million hESC-derived OPCs was not significantly ($p > 0.1$) different from those that received 250,000 hESC-derived OPCs, as determined using the BBB locomotor rating scale. ***c***, Animals that received hESC-derived OPCs also exhibited significant increases in locomotor recovery as determined using four-parameter kinematic analyses.

were detected throughout the transverse plane of the spinal cord, primarily within the gray matter near the site of implantation and within gray and white matter away from the site of implantation. Bisbenzimide-positive, BrdU-positive, and anti-human nuclei-positive cells were absent in nontransplanted animals. Quantitative analysis indicated that BrdU-positive cells were detected 11 mm cranial and 1 mm caudal to the site of implantation, with the greatest number of cells around the site of implantation in most animals and only a modest number of im-

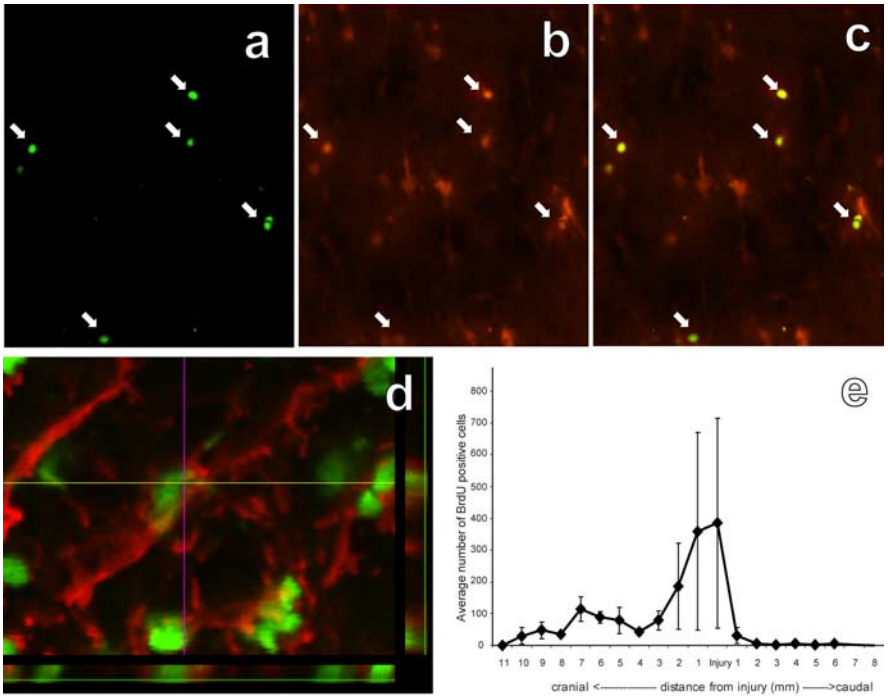

Figure 6. Chronic transplantation of hESC-derived OPCs resulted in cell survival, limited redistribution from the site of implantation, and differentiation to mature oligodendrocytes. ***a***, Anti-BrdU-positive OPCs (arrows) double labeled with the mature oligodendrocyte marker APC-CC1 (arrows; ***b***); a composite is shown in ***c***. ***d***, Anti-BrdU-positive, APC-CC1-positive double labeling was confirmed using 3-D reconstruction of confocally scanned thin-plane images. ***e***, Distribution of total numbers of BrdU-prelabeled cells within spinal cord transverse sections 2 months after transplantation and 10 months after SCI. Error bars illustrate SD. Magnification: ***a–c***, 400×; ***d***, 2000×.

planted cells redistributed over long distances (Fig. 6*e*). Notably, the number of cells around the implantation site varied among animals in the chronic transplantation group (Fig. 6*e*).

Immunohistochemical staining identified anti-human nuclei-positive cells, bisbenzimide-positive cells, and BrdU-positive cells (Fig. 6*a*) that double labeled with the oligodendroglial marker APC-CC1 (Fig. 6*b*,*c*), indicating that transplanted cells differentiated into oligodendrocytes. Double labeling was confirmed using 3-D reconstruction of confocally scanned thin-plane images (Fig. 6*d*). In all instances, double-labeled cells were found in clusters. Both transplanted and nontransplanted animals contained APC-CC1-positive cells that were anti-human nuclei-negative, bisbenzimide-negative, and BrdU-negative, indicating endogenous oligodendrocytes. No anti-human nuclei-positive, BrdU-positive, or bisbenzimide-positive cells colabeled with GFAP or NeuN.

OPCs do not remyelinate axons or improve locomotion when transplanted at 10 months after injury

Although transplanted OPCs survived in the chronic injury sites, transplantation did not alter the state of myelination (Fig. 7). Regions of pathology contained normally myelinated and demyelinated axons, with no discernable difference in remyelinated axons (compare Figs. 4*b* and 7*a*, illustrating robust remyelination after acute transplantation). Demyelinated and myelinated axons were present at 10 months after injury (Fig. 7*b*,*c*), surrounded by enlarged intermediate filament-rich astrocytic processes, which occupied virtually all of the extracellular space (Fig. 7*c*,*d*). Astrocyte cell bodies with enlarged intermediate filament-rich astrocytic processes were abundant (Fig. 7*d*).

Consistent with the qualitative evidence for a lack of remyelination, quantitative analyses indicated that the density of oligodendrocyte remyelinated axons was not significantly different ($p > 0.1$) in OPC-transplanted animals compared with control animals (Fig. 7*e*). Quantification of normally myelinated, demyelinated, and Schwann cell-remyelinated axons within the chronic transplant group indicated that these axon densities were also not significantly different ($p > 0.1$) than in control animals (Fig. 7*e*). Notably, a comparison of the density of demyelinated axons in the chronic nontransplanted control group (Fig. 7*e*) and the acute nontransplanted control group (Fig. 4*f*) indicates that the density of demyelinated axons increases significantly ($p < 0.01$) over time. Endogenous remyelination also increased significantly ($p < 0.01$) over time; the total number of oligodendrocyte and Schwann cell-remyelinated axons in nontransplanted control animals increased from 7592/mm^2 at 2 months after injury (Fig. 4*f*) to 13,026/mm^2 at 12 months after injury (Fig. 7*e*), indicating a 72% increase in endogenous remyelination over time.

Transplantation of hESC-derived OPCs 10 months after SCI resulted in no significant ($p > 0.1$) improvement in locomotor abilities compared with control animals, regardless of the severity of injury (Fig. 7*f–h*). Indeed, locomotor function was remarkably stable at a level that was impaired relative to uninjured controls (normal BBB score, 21). Both the transplanted and control animal groups in the chronic study showed greater variability in injury response than animals in the acute study. However, the variability of BBB scores at 30 d after injury for the transplanted (±5) and control (±5) chronic study groups was not significantly different ($p > 0.1$) from the variability of BBB scores at 382 d after injury for the transplanted (±5) and control (±5) groups. These data indicate that by 1 month after injury, animals reach a plateau in their locomotor recovery that does not change over the year-long experiment; this finding is also supported by the following analysis. This chronic study involved treating animals at 10 months after injury or ~9 months after they had reached a plateau in their locomotor abilities. This provided the opportunity to compare pretreatment and posttreatment BBB scores for individual animals. We determined the variance of the BBB scores for each animal in the transplanted and control groups from the point of plateau in their locomotor abilities at 30 d after injury until the end of the experiment at 382 d after injury. The range of variance for the transplant group was 0.54–0.68, and the range of variance for the control group was 0.52–0.71. A comparison of the variance (*t* test) of all animals in the transplanted group with all animals in the control group indicated no significant difference ($p > 0.1$). These data indicate that there is no significant change in BBB before and after treatment for any single animal in either the transplant or control group or in either group as a whole.

Improved locomotion after acute transplantation is not attributable to enhanced tissue sparing

To assess the possibility that OPC transplantation caused tissue sparing, we examined the gross morphology of the injured spinal

cord and the extent of tissue sparing/loss using morphometric analyses. Light microscopic examination of spinal cord cross sections at 1 mm intervals indicated that injured animals that received DMEM injections consistently demonstrated cavitation extending several millimeters from the injury site (Fig. 8*a–c*). In contrast, both hFb- and OPC-transplanted animals had little or no cavitation, although there was an extensive loss of central gray matter (Fig. 8*d–f*). Because cavitation was reduced in both the OPC- and hFb-transplanted groups, whereas improved locomotion was seen in only the OPC-transplanted group, the reduction in cavitation is not the cause of the improved locomotion in OPC-transplanted animals.

Similarly, direct morphometric analysis of the acute transplant groups indicated that the degree of tissue sparing did not differ between animals that received OPC or hFb transplants [i.e., cross-sectional areas in OPC-transplanted animals were not significantly different ($p > 0.1$) from those in hFb-transplanted controls] (Fig. 8*g*). Both OPC-transplanted and hFb-transplanted groups did have significantly greater ($p < 0.01$) cross-sectional areas than vehicle-only controls at 1 and 2 mm cranial to the injury epicenter. Again, because tissue sparing was enhanced in both the OPC- and hFb-transplanted groups, whereas improved locomotion was seen in only the OPC-transplanted group, the enhanced tissue sparing is not the cause of improved locomotion in OPC-transplanted animals.

A significantly greater ($p < 0.01$) cross-sectional area was also apparent at 1 mm caudal to the lesion epicenter in animals transplanted with OPCs 10 months after SCI compared with DMEM-injected controls (Fig. 8*h*), providing another example of the dissociation between enhanced tissue sparing and enhanced recovery.

We did not observe tumor, teratoma, or non-neuronal tissue formation in transplant recipients.

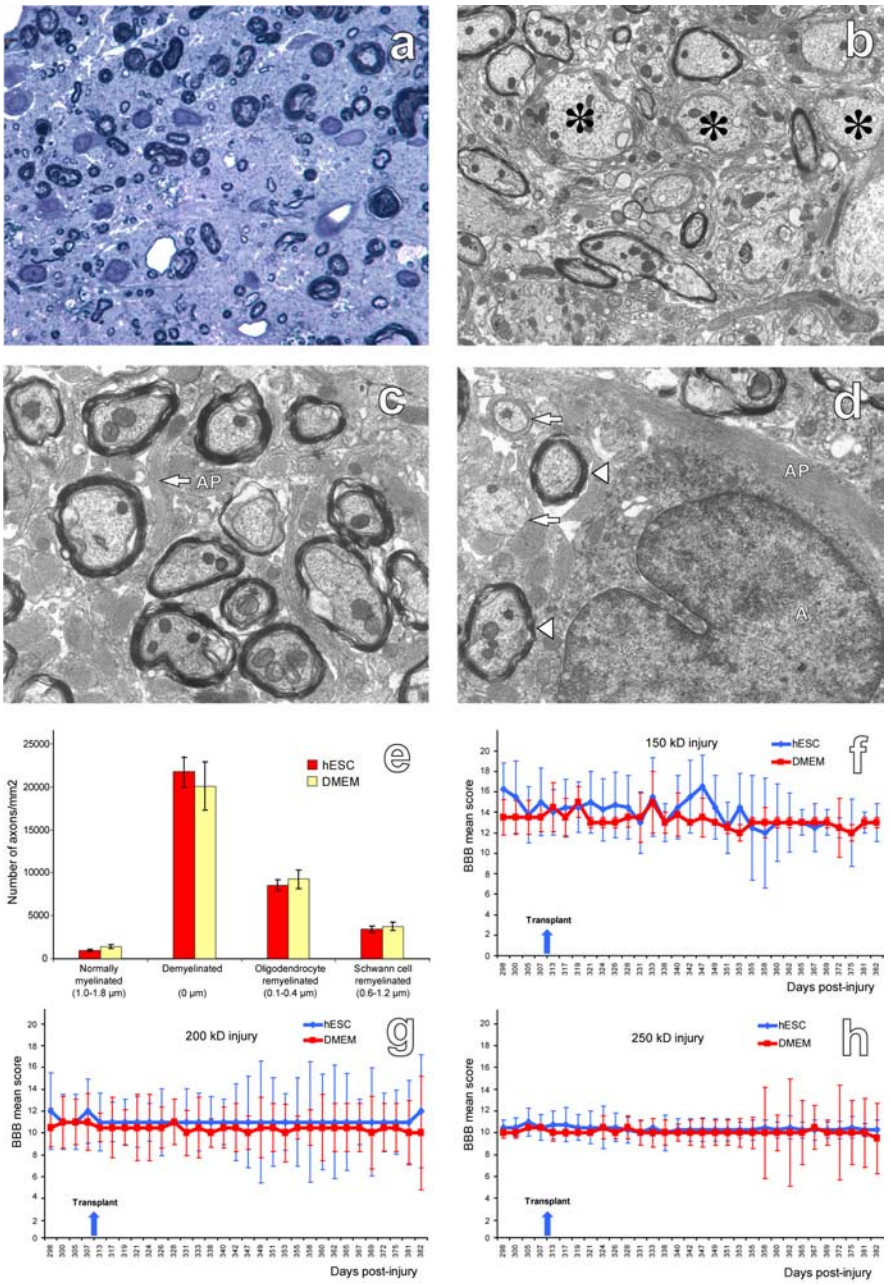

Figure 7. Chronic transplantation of hESC-derived OPCs resulted in no change in the density of oligodendrocyte remyelination or locomotor recovery compared with controls. ***a***, Toluidine blue-stained transverse section from a transplanted animal, illustrating very sparse remyelination among normally myelinated and demyelinated axons, and increased extracellular space. ***b***, Electron micrograph of the transplant environment at 10 months after injury, illustrating that demyelinated axons (*) were present. ***c***, Electron micrograph of the transplant environment at 10 months after injury, illustrating axons surrounded by enlarged intermediate filament-rich astrocytic processes (AP), which occupied virtually all of the extracellular space. ***d***, Electron micrograph of the transplant environment at 10 months after injury, illustrating an astrocyte (***a***) with a large intermediate filament-rich process (AP) extending to demyelinated axons surrounded by intermediate filament-rich astrocytic processes (arrows) and myelinated axons surrounded by intermediate filament-rich astrocytic processes (arrowheads). ***e***, Quantification of normally myelinated, demyelinated, and oligodendrocyte or Schwann cell-remyelinated axons in hESC-derived OPC transplanted, and DMEM-injected animals. Error bars illustrate SD. The myelin sheath thickness for each class of axons is indicated in brackets. ***f–h***, The degree of locomotor recovery in animals that received 1.5 million cell transplants was not significantly ($p > 0.1$) different from those that received vehicle-only injections, regardless of the severity of injury. Magnification: ***a***, 400×; ***b–d***, 3000×.

Discussion

Demyelination of intact axons is a prominent feature of SCI (Totoiu and Keirstead, 2005) and is an important contributor to functional loss in many CNS disorders, including trauma, multiple sclerosis (MS), and stroke (Gledhill et al., 1973; Blight, 1985; Bunge et al., 1993). This report demonstrates for the first time that targeting demyelination is a viable therapeutic strategy for restoration of function after SCI and is the first to do so using human embryonic stem cells in a cellular replacement strategy. Importantly, our data also indicate that the therapeutic window for this type of treatment is limited to the early postinjury period.

The importance of cell-type specification for cell-replacement strategies

One of the greatest challenges facing hESC research is the derivation of high-purity lineages from pluripotent hESCs. This is critical because of the potential of pluri-potent cells to differentiate

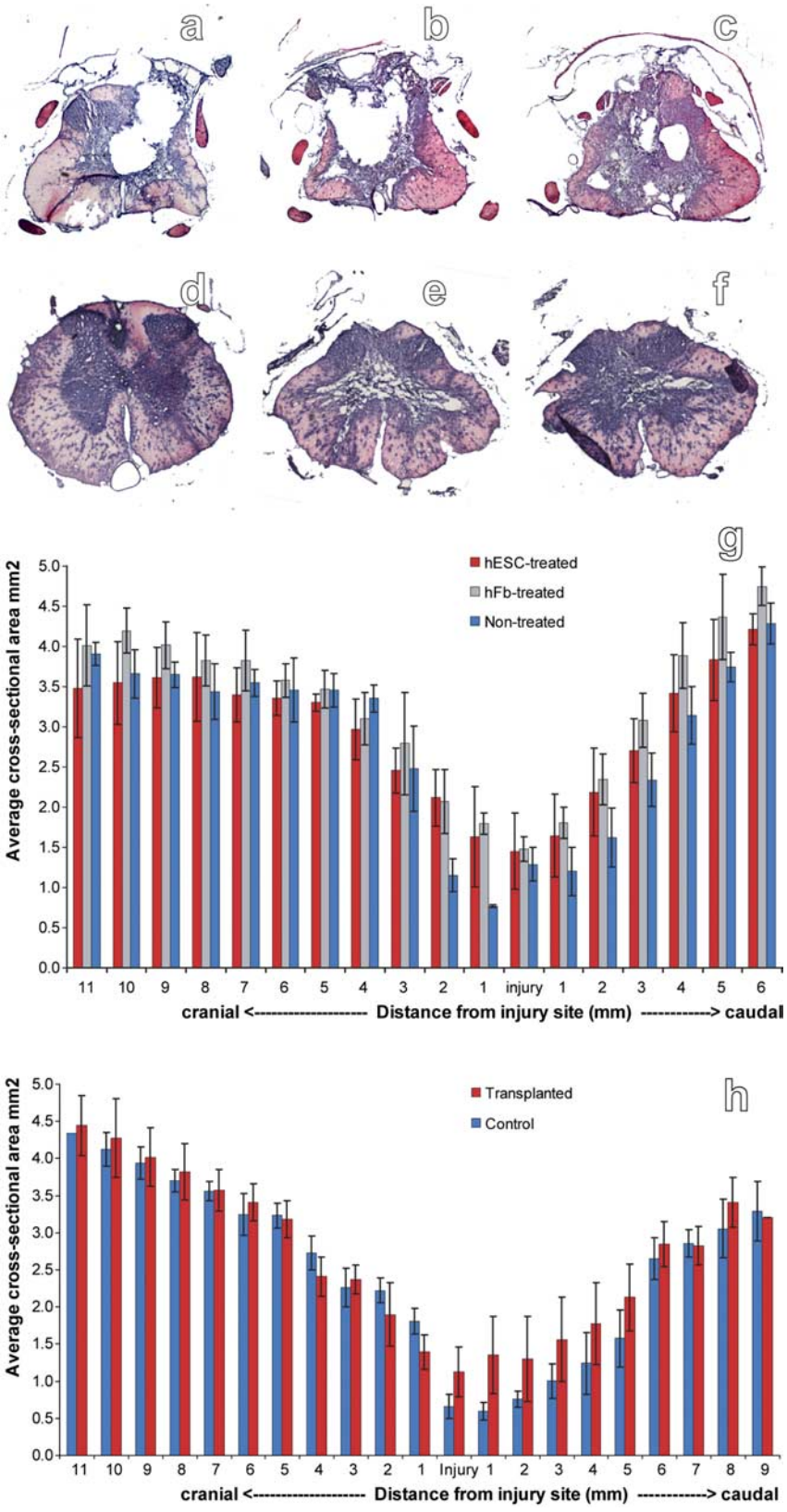

Figure 8. Morphometric analysis indicated that transplantation of hESC-derived OPCs 1 week or 10 months after SCI decreased cavitation but did not alter the extent of tissue sparing or tissue loss. Animals receiving vehicle-only consistently demonstrated cavitation at 1 mm cranial to the injury epicenter (***a***), at the epicenter (***b***), and 1 mm caudal to the injury epicenter (***c***). Animals receiving either OPC transplants consistently demonstrated little or no cavitation at 1 mm cranial to the injury epicenter (***d***), at the epicenter (***e***), and 1 mm caudal to the injury epicenter (***f***). Morphometric analyses at 1 mm intervals through the spinal cord indicated that transplantation of OPCs 7 d (***g***) or 10 months (***h***) after SCI did not cause overt tissue sparing or tissue loss. Error bars illustrate SD. Magnification: ***a–f***, 10×.

into teratomas. Research of hESC differentiation benefits from two decades of mouse stem cell research, which has provided us with methods to differentiate mouse stem cells into several clinically relevant neural (Deacon et al., 1998; Brustle et al., 1999; Lee et al., 2000; Liu et al., 2000; Kim et al., 2003) and non-neural (Wiles and Keller, 1991; Klug et al., 1996; Soria et al., 2000) cell types. Neurons and glia have also been derived from neural stem cells isolated from the fetal human brain (Keyoung et al., 2001). Although hESCs have been directed to differentiate into multipotent neural precursors (Carpenter et al., 2001; Reubinoff et al., 2001; Zhang et al., 2001; Li et al., 2005), the differentiation protocol that we used here is unique in that it generates a highly purified, specific neural cell type, OPCs (Nistor et al., 2005). This provided us with a novel tool to investigate the ability of these cells to remyelinate regions of SCI and determine whether remyelination confers functional benefit after SCI.

The present results reveal that the hESCs that had been differentiated into OPCs survived, differentiated into oligodendrocytes, and redistributed over short distances of the spinal cord during the postimplantation survival period, whether transplanted 1 week or 10 months after SCI. No transplanted cells displayed antigenic markers characteristic of astrocytes or neurons. This finding, together with the *in vitro* immunocytochemical profiling of the transplant population, indicates effective predifferentiation of cells to the oligodendroglial lineage and a lack of reversion to a more pluri-potent phenotype after transplantation to an injury site. Such characteristics are crucial if hESCs are to be useful for tissue repair.

The therapeutic window for remyelination and functional benefit is limited to the early postinjury interval

Transplantation of hESC-derived OPCs 1 week after SCI resulted in widespread oligodendrocyte remyelination throughout the white matter. The total number of remyelinated axons in this transplant group increased by 136% compared with endogenous remyelination in controls. Remyelination in the acute OPC-transplanted group was approximately double the amount of endogenous remyelination that occurred over the year after injury in non-transplanted controls, which increased by 72% from 2–12 months after injury. Ensheathment of axons by processes of GFP-positive-transplanted cells confirmed that some remyelination was performed by

transplanted OPCs, although we cannot rule out the possibility that OPC transplantation also enhanced remyelination by endogenous oligodendrocytes. Rodent stem cell-derived glial precursors have previously been shown to myelinate after transplantation into the myelin-deficient rat (Brustle et al., 1999), and rodent neural precursor-derived glial-committed progenitors (Ben-Hur et al., 1998; Keirstead et al., 1999) have been shown to myelinate after transplantation into regions of acute experimental demyelination (Keirstead et al., 1999) as well as the mouse hepatitis virus model of multiple sclerosis (Totoiu et al., 2004). In addition, McDonald et al. (1999) reported that transplantation of neural differentiated mouse embryonic stem cells into rat spinal cord injury sites improved functional recovery and suggested remyelination as a likely mechanism underlying the effect. The present study is the first to show that remyelination-competent cells can also be derived from human stem cells, and that these cells can be used in a spinal cord injury context.

Transplantation of hESC-derived OPCs 10 months after SCI did not result in increased remyelination compared with control animals that did not receive OPCs. Pathological analysis of the chronic transplant group indicated widespread astrogliosis and engulfment of axons by astrocyte processes. Virtually all axons in this animal group, regardless of their state of myelination, were surrounded by astrocyte processes. The failure of transplanted OPCs to remyelinate chronic spinal cord injuries is particularly intriguing in light of the significantly higher density of demyelinated axons compared with the acute injury group. The increase over time in the density of demyelinated axons supports previous studies that illustrate that spinal cord injury is accompanied by delayed apoptosis of oligodendrocytes (Crowe et al., 1997) and progressive demyelination (Totoiu and Keirstead, 2005). The inability of a myelinogenic transplant population to remyelinate denuded axons in chronic injury sites suggests that an inhibitor of remyelination is present in these sites.

Several reports in the literature indicate that the failure of remyelination can be correlated to the presence of an astroglial scar. A profound example is found in the pathology of chronic MS plaques, which are characterized by robust astrogliosis and an absence of remyelination; this is in contrast to acute MS lesions in which an absence of sclerosis is correlated with widespread remyelination (Wu and Raine, 1992; Lucchinetti et al., 1996; Raine, 1997). A correlation between astrogliosis and persistent demyelination has also been made in the lesioned adult rat anterior medullary velum (Butt and Berry, 2000), the demyelinated guinea pig optic nerve (Sergott et al., 1985), the cuprizone (Hiremath et al., 1998), and experimental allergic encephalomyelitis (Linington et al., 1992) model of demyelination, the hypomyelinating taiep mutant rat (Krsulovic et al., 1999), and dysmyelinating mutant mice (Jacque et al., 1986). These studies, together with the observation that remyelination can occur in the presence of reactive astrocytes (Triarhou and Herndon, 1985), suggest that established but not necessarily ongoing astrogliosis contributes to the failure of remyelination. Our findings extend these studies by demonstrating that progressive astrogliosis after SCI correlates with a loss of the ability of a myelinogenic transplant population to effect remyelination. Nonetheless, other inhibitors of remyelination, including an inappropriate growth factor milieu, extracellular matrix scarring, and an OPC-directed immune response, may also contribute to the failure of remyelination after transplantation into chronic spinal cord injury sites.

Locomotor ability significantly improved beyond controls only in those animals transplanted 1 week after SCI that contained robust remyelination. Animals transplanted 10 months after SCI demonstrated no remyelination and no significant improvement in locomotor ability. The persistence of cells throughout the survival period in both acute and chronically transplanted animals indicate that a nonspecific effect of cell transplantation/survival on endogenous cells is not a likely contributor to the locomotor improvement. Likewise, the findings that both acute OPC-transplanted and hFb-transplanted groups demonstrated cross-sectional areas that were greater than vehicle-only controls, but only the OPC-transplanted group demonstrated behavioral improvement, indicates that tissue sparing was not a likely contributor to the locomotor improvement. Together, these findings suggest that remyelination was responsible for the locomotor improvement and support the observation that remyelination can restore saltatory conduction (Smith et al., 1979; Utzschneider et al., 1994; Waxman et al., 1994) and locomotor deficits (Jeffery and Blakemore, 1997; Jeffery et al., 1999) in experimental models of demyelination. Nonetheless, we cannot rule out the possibility that locomotor improvement may have resulted from an uncharacterized effect of the transplant, such as neurotrophin-induced axonal sprouting (Lu et al., 2003).

These studies demonstrate that transplantation of hESCs predifferentiated to an oligodendroglial lineage is an effective strategy for the treatment of acute SCI and underscore the importance of myelination as a therapeutic target. Furthermore, these studies suggest that the therapeutic window of opportunity for remyelination and functional locomotor improvement after cell transplantation into SCI sites is dictated by the astroglial histopathology of white matter tracts. Identification of astrogliosis as a critical determinant of remyelination success after SCI would extend the inhibitory role of this pathological process beyond axonal extension, cellular migration, and remyelination of demyelinating disorders such as MS.

References

Basso DM, Beattie MS, Bresnahan JC (1995) A sensitive and reliable locomotor rating scale for open field testing in rats. J Neurotrauma 12:1–21.

Ben-Hur TRB, Murray K, Rougon G, Dubois-Dalcq M (1998) Growth and fate of PSA-NCAM+ precursors of the postnatal brain. J Neurosci 18:5777–5788.

Blight AR (1983) Cellular morphology of chronic spinal cord injury in the cat: analysis of myelinated axons by line-sampling. Neuroscience 10:521–543.

Blight AR (1985) Delayed demyelination and macrophage invasion: a candidate for secondary cell damage in spinal cord injury. Cent Nerv Syst Trauma 2:299–315.

Brustle O, Spiro AC, Karram K, Choudhary K, Okabe S, McKay RD (1997) In vitro-generated neural precursors participate in mammalian brain development. Proc Natl Acad Sci USA 94:14809–14814.

Brustle O, Jones KN, Learish RD, Karram K, Choudhary K, Wiestler OD, Duncan ID, McKay RD (1999) Embryonic stem cell-derived glial precursors: a source of myelinating transplants. Science 285:754–756.

Bunge RP, Puckett WR, Becerra JL, Marcillo A, Quencer RM (1993) Observations on the pathology of human spinal cord injury. A review and classification of 22 new cases with details from a case of chronic cord compression with extensive focal demyelination. Adv Neurol 59:75–89.

Butt AM, Berry M (2000) Oligodendrocytes and the control of myelination in vivo: new insights from the rat anterior medullary velum. J Neurosci Res 59:477–488.

Carpenter MK, Inokuma MS, Denham J, Mujtaba T, Chiu CP, Rao MS (2001) Enrichment of neurons and neural precursors from human embryonic stem cells. Exp Neurol 172:383–397.

Crowe MJ, Bresnahan JC, Shuman SL, Masters JN, Beattie MS (1997) Apoptosis and delayed degeneration after spinal cord injury in rats and monkeys. Nat Med 3:73–76.

Deacon T, Dinsmore J, Costantini LC, Ratliff J, Isacson O (1998) Blastula-

stage stem cells can differentiate into dopaminergic and serotonergic neurons after transplantation. Exp Neurol 149:28–41.
Gilson JM, Blakemore WF (2002) Schwann cell remyelination is not replaced by oligodendrocyte remyelination following ethidium bromide induced demyelination. NeuroReport 13:1205–1208.
Gledhill RF, Harrison BM, McDonald WI (1973) Demyelination and remyelination after acute spinal cord compression. Exp Neurol 38:472–487.
Gonzalez R, Glaser J, Liu MT, Lane TE, Keirstead HS (2003) Reducing inflammation decreases secondary degeneration and functional deficit after spinal cord injury. Exp Neurol 184:456–463.
Guy J, Ellis EA, Kelley K, Hope GM (1989) Spectra of G ratio, myelin sheath thickness, and axon and fiber diameter in the guinea pig optic nerve. J Comp Neurol 287:446–454.
Heins N, Malatesta P, Cecconi F, Nakafuku M, Tucker KL, Hack MA, Chapouton P, Barde YA, Gotz M (2002) Glial cells generate neurons: the role of the transcription factor Pax6. Nat Neurosci 5:308–315.
Hildebrand C, Hahn R (1978) Relation between myelin sheath thickness and axon size in spinal cord white matter of some vertebrate species. J Neurol Sci 38:421–434.
Hiremath MM, Saito Y, Knapp GW, Ting JP, Suzuki K, Matsushima GK (1998) Microglial/macrophage accumulation during cuprizone-induced demyelination in C57BL/6 mice. J Neuroimmunol 92:38–49.
Jacque C, Rolland B, Caldani M, Fages C, Tardy M (1986) Absence of correlations between glutamine-synthetase activity and dysmyelination-associated modifications of astroglia in the brain of murine mutants. Neurochem Res 11:527–533.
Jeffery ND, Blakemore WF (1997) Locomotor deficits induced by experimental spinal cord demyelination are abolished by spontaneous remyelination. Brain 120:27–37.
Jeffery ND, Crang AJ, O'Leary MT, Hodge SJ, Blakemore WF (1999) Behavioural consequences of oligodendrocyte progenitor cell transplantation into experimental demyelinating lesions in the rat spinal cord. Eur J Neurosci 11:1508–1514.
Kakulas BA (1999) The applied neuropathology of human spinal cord injury. Spinal Cord 37:79–88.
Keirstead HS, Ben-Hur T, Rogister B, O'Leary MT, Dubois-Dalcq M, Blakemore WF (1999) Polysialylated neural cell adhesion molecule-positive CNS precursors generate both oligodendrocytes and Schwann cells to remyelinate the CNS after transplantation. J Neurosci 19:7529–7536.
Keyoung HM, Roy NS, Benraiss A, Louissaint Jr A, Suzuki A, Hashimoto M, Rashbaum WK, Okano H, Goldman SA (2001) High-yield selection and extraction of two promoter-defined phenotypes of neural stem cells from the fetal human brain. Nat Biotechnol 19:843–850.
Kim JY, Koh HC, Lee JY, Chang MY, Kim YC, Chung HY, Son H, Lee YS, Studer L, McKay R, Lee SH (2003) Dopaminergic neuronal differentiation from rat embryonic neural precursors by Nurr1 overexpression. J Neurochem 85:1443–1454.
Klug MG, Soonpaa MH, Koh GY, Field LJ (1996) Genetically selected cardiomyocytes from differentiating embryonic stem cells form stable intracardiac grafts. J Clin Invest 98:216–224.
Krsulovic J, Couve E, Roncagliolo M (1999) Dysmyelination, demyelination and reactive astrogliosis in the optic nerve of the taiep rat. Biol Res 32:253–262.
Lee SH, Lumelsky N, Studer L, Auerbach JM, McKay RD (2000) Efficient generation of midbrain and hindbrain neurons from mouse embryonic stem cells. Nat Biotechnol 18:675–679.
Li XJ, Du ZW, Zarnowska ED, Pankratz M, Hansen LO, Pearce RA, Zhang SC (2005) Specification of motoneurons from human embryonic stem cells. Nat Biotechnol 23:215–221.
Linington C, Engelhardt B, Kapocs G, Lassman H (1992) Induction of persistently demyelinated lesions in the rat following the repeated adoptive transfer of encephalitogenic T cells and demyelinating antibody. J Neuroimmunol 40:219–224.
Liu S, Qu Y, Stewart TJ, Howard MJ, Chakrabortty S, Holekamp TF, McDonald JW (2000) Embryonic stem cells differentiate into oligodendrocytes and myelinate in culture and after spinal cord transplantation. Proc Natl Acad Sci USA 97:6126–6131.
Lu P, Jones LL, Snyder EY, Tuszynski MH (2003) Neural stem cells constitutively secrete neurotrophic factors and promote extensive host axonal growth after spinal cord injury. Exp Neurol 181:115–129.
Lucchinetti CF, Bruck W, Rodriguez M, Lassmann H (1996) Distinct patterns of multiple sclerosis pathology indicates heterogeneity on pathogenesis. Brain Pathol 6:259–274.
McDonald JW, Liu XZ, Qu Y, Liu S, Mickey SK, Turetsky D, Gottlieb DI, Choi DW (1999) Transplanted embryonic stem cells survive, differentiate and promote recovery in injured rat spinal cord [see comments]. Nat Med 5:1410–1412.
Nashmi R, Fehlings MG (2001) Mechanisms of axonal dysfunction after spinal cord injury: with an emphasis on the role of voltage-gated potassium channels. Brain Res Brain Res Rev 38:165–191.
Nistor GI, Totoiu MO, Haque N, Carpenter MK, Keirstead HS (2005) Human embryonic stem cells differentiate into oligodendrocytes in high purity and myelinate after spinal cord transplantation. Glia 49:385–396.
Okabe S, Forsberg-Nilsson K, Spiro AC, Segal M, McKay RD (1996) Development of neuronal precursor cells and functional postmitotic neurons from embryonic stem cells in vitro. Mech Dev 59:89–102.
Raine CS (1997) The Norton lecture: a review of the oligodendrocyte in the multiple sclerosis lesion. J Neuroimmunol 77:135–152.
Reubinoff BE, Itsykson P, Turetsky T, Pera MF, Reinhartz E, Itzik A, Ben-Hur T (2001) Neural progenitors from human embryonic stem cells. Nat Biotechnol 19:1134–1140.
Sergott RC, Brown MJ, Polenta RM, Lisak RP, Silberberg DH (1985) Optic nerve demyelination induced by human serum: patients with multiple sclerosis or optic neuritis and normal subjects. Neurology 35:1438–1442.
Smith EJ, Blakemore WF, McDonald WI (1979) Central remyelination restores secure conduction. Nature 280:395–396.
Soria B, Roche E, Berna G, Leon-Quinto T, Reig JA, Martin F (2000) Insulin-secreting cells derived from embryonic stem cells normalize glycemia in streptozotocin-induced diabetic mice. Diabetes 49:157–162.
Thomson JA, Itskovitz-Eldor J, Shapiro SS, Waknitz MA, Swiergiel JJ, Marshall VS, Jones JM (1998) Embryonic stem cell lines derived from human blastocysts. Science 282:1145–1147.
Totoiu MO, Keirstead HS (2005) Spinal cord injury is accompanied by chronic progressive demyelination. J Comp Neurol, in press.
Totoiu MO, Nistor GI, Lane TE, Keirstead HS (2004) Remyelination, axonal sparing, and locomotor recovery following transplantation of glial-committed progenitor cells into the MHV model of multiple sclerosis. Exp Neurol 187:254–265.
Triarhou LC, Herndon RM (1985) Effect of macrophage inactivation on the neuropathology of lysolecithin-induced demyelination. Br J Exp Pathol 66:293–301.
Utzschneider DA, Archer DR, Kocsis JD, Waxman SG, Duncan ID (1994) Transplantation of glial cells enhances action potential conduction of amyelinated spinal cord axons in the myelin-deficient rat. Proc Natl Acad Sci USA 91:53–57.
Waxman SG, Utzschneider DA, Kocsis JD (1994) Enhancement of action potential conduction following demyelination: experimental approaches to restoration of function in multiple sclerosis and spinal cord injury. Prog Brain Res 100:233–243.
Wiles MV, Keller G (1991) Multiple hematopoietic lineages develop from embryonic stem (ES) cells in culture. Development 111:259–267.
Wu E, Raine CS (1992) Multiple sclerosis. Interactions between oligodendrocytes and hypertrophic astrocytes and their occurrence in other, non-demyelinating conditions. Lab Invest 67:88–99.
Zhang SC, Wernig M, Duncan ID, Brustle O, Thomson JA (2001) In vitro differentiation of transplantable neural precursors from human embryonic stem cells. Nat Biotechnol 19:1129–1133.